Mount St. Helens—Controlled-Source Audio-Frequency Magnetotelluric (CSAMT) Data and Inversions

Spirit Lake

Mount St. Helens

Crater Glacier

Crater rim

Data Series 901

©2014Google

Mount St. Helens—Controlled-Source Audio-Frequency Magnetotelluric (CSAMT) Data and Inversions

By Jeff Wynn and Herbert A. Pierce

U.S. Department of the Interior
SALLY JEWELL, Secretary

U.S. Geological Survey
Suzette M. Kimball, Acting Director

U.S. Geological Survey, Reston, Virginia: 2015

Contents

Figures

Tables

Mount St. Helens—Controlled-Source Audio-Frequency Magnetotelluric (CSAMT) Data and Inversions

By Jeff Wynn and Herbert A. Pierce

Introduction

This report describes a series of geoelectrical soundings carried out on and near Mount St. Helens volcano, Washington, in 2010–2011. These soundings used a controlled-source audio-frequency magnetotelluric (CSAMT) approach (Zonge and Hughes, 1991; Simpson and Bahr, 2005). We chose CSAMT for logistical reasons: It can be deployed by helicopter, has an effective depth of penetration of as much as 1 kilometer, and requires less wire than a Schlumberger sounding.

This Data Series provides the edited data for these CSAMT soundings as well as several different types of 1-D inversions (where the signal data are converted to conductivity-versus-depth models). In addition, we include a map showing station locations on and around the volcano and the Pumice Plain to the north.

The apparent conductivity (or its inverse, apparent resistivity) measured by a geoelectrical system is caused by several factors. The most important of these are water-filled rock porosity and the presence of water-filled fractures; however, rock type and minerals (for instance, sulfides and clay content) also contribute to apparent conductivity. In situations with little recharge (for instance, in arid regions), variations in ionic content of water occupying pore space and fractures sampled by the measurement system must also be factored in (Wynn, 2006). Variations in ionic content may also be present in hydrothermal fluids surrounding volcanoes in wet regions. In unusual cases, temperature may also affect apparent conductivity (Keller, 1989; Palacky, 1989). There is relatively little hydrothermal alteration (and thus fewer clay minerals that might add to the apparent conductivity) in the eruptive products of Mount St. Helens (Reid and others, 2010), so conductors observed in the Fischer, Occam, and Marquardt inversion results later in this report are thus believed to map zones with significant water content. Geoelectrical surveys thus have the potential to reveal subsurface regions with significant groundwater content, including perched and regional aquifers. Reid and others (2001) and Reid (2004) have suggested that groundwater involvement may figure in both the scale and the character of some if not all volcanic edifice collapse events. Ongoing research by the U.S. Geological Survey (USGS) and others aims to better understand the contribution of groundwater to both edifice pore pressure and rock alteration as well as its direct influence on eruption processes by violent interaction with magma (Schmincke, 1998).

Data Acquisition

The CSAMT soundings were carried out using a Geometrics Stratagem EH-4 system on and near Mount St. Helens in 2010 and 2011. In all cases save one (station MSH-1102, where a natural-source audio-frequency magnetotelluric [NSAMT] approach was used), a controlled-source inductive transmitter was used to improve the quality of the received signal. The transmitter substantially improves the signal/noise ratio and thus shortens the time required for a measurement. Station MSH-1102 (NSAMT) was repeated using a controlled-source electromagnetic transmitter, with station MSH-1110 (CSAMT) measured subsequently as a quality check. The transmitter was always located approximately 250 meters away from each receiver location to maximize signal quality, but also to avoid near-field distortion effects. The transmitter was only needed to augment the weak mid-band natural signals (450–2,700 Hz), so we acquired preliminary bulk resistivity data and used the Stratagem EH-4 manual (Geometrics, 2007, fig. 5) to calculate skin-depth and guide us on where to place the transmitter. We used high-sensitivity EMI Corporation magnetic coils and orthogonal, 25-meter electric dipoles. The latter were coupled to porous-pot ceramic, non-polarizing electrodes, as sensors. The CSAMT station locations are shown in figure 1, and the station coordinates and elevations are provided in the "GPS Data" section (table 1). Photographs of the CSAMT equipment are shown in figure 2. A Long Ranger (Bell 206L) helicopter was used for access to all stations, with permission of the Mount St. Helens National Volcanic Monument. Two load trips were required for each station.

Figure 1.   A Google Earth image of Mount St. Helens, showing the controlled-source audio-frequency magnetotelluric (CSAMT) station locations. The step scarp, a pronounced topographic offset (north side down), is shown as a blue line.

Figure 2. Images showing data acquisition. *A*, The controlled-source audio-frequency magnetotelluric (CSAMT) transmitter for repeat station MSH-1001-1002, located north of Crater Glacier (black ridge visible in the middle distance) and the 1980–86 and 2004–2008 dacite lava domes (left upper background) inside Mount St. Helens crater (crater walls seen in the top center and upper right). USGS photograph by Jeff Wynn. *B*, The first author with the Stratagem EH-4 controlled-source audio-frequency magnetotelluric (CSAMT) receiver and the electrodes used for the electrical-field measurements. The location here is station MSH-1001-1002, just north of Crater Glacier (seen in the background behind the umbrella). USGS photo by Tami Christensen.

Table 1. GPS coordinates and elevations for the controlled-source audio-frequency magnetotelluric (CSAMT) stations acquired in and adjacent to Mount St. Helens, Washington. (Datum: WGS 84)

[Coordinates given represent CSAMT receiver locations. The transmitter was located ~250 meters away. Stations 1001/1002 were repeats using the same transmitter-receiver locations. Stations 1003/1004 were repeats using the same transmitter-receiver locations. Stations 1001–1004 were acquired north of and near the toe of the Mount St. Helens Glacier on September 14, 2010. Stations 1102 & 1110 were acquired on separate days using close but not identical transmitter-receiver locations. Stations 1102 & 1110 were acquired very close to the toe of the Mount St. Helens Glacier on September 6 and 7, 2011.]

Station	UTM zone 10N		Latitude	Longitude	Surface elevation	
	Northing	Easting			(ft)	(m)
2010						
MSH-1001/2	5117961	562593	46.212	-122.189	5570	1698
MSH-1003/4	5118187	562600	46.214	-122.188	5496	1675
2011						
MSH-1102	5117948	562577	46.212	-122.189	5597	1706
MSH-1103	5118806	562640	46.222	-122.188	5017	1530
MSH-1104	5119891	562818	46.232	-122.185	4035	1230
MSH-1105	5120906	562821	46.241	-122.185	3762	1147
MSH-1106	5122024	562873	46.251	-122.184	3634	1108
MSH-1107	5113516	563243	46.174	-122.181	5622	1714
MSH-1108	5116637	559491	46.203	-122.229	5004	1526
MSH-1109	5116186	564853	46.198	-122.159	6022	1836
MSH-1110	5117948	562587	46.212	-122.189	5590	1704

2010

The soundings carried out in September 2010 were done as a proof-of-concept experiment. They successfully identified a shallow conductor seen earlier in time-domain electromagnetic (TEM) profiling carried out in 2007 (Bedrosian and others, 2008). The soundings represent two repeat measurements each at two different receiver locations inside the crater, and close to the terminus of the growing Crater Glacier at that time. The double measurements were made to ascertain the precision that we could anticipate during subsequent measurements and inversions of the data. Two different receiver locations (see next section) were utilized with an equidistant transmitter for all four measurements. The 2010 stations are labeled MSH-1001 to MSH-1004.

2011

Additional soundings were carried out in September 2011 in two stages. Environmental conditions were virtually identical both years. The first stage acquired a profile from the terminus of the Crater Glacier to the North Fork Toutle River, crossing and sampling the Pumice Plain in a north-south transect. This profile was designed to map the deep regional aquifer, and to determine what (if any) connection it had to the shallow aquifer observed a year earlier inside the crater. Three additional stations were acquired subsequently on the south, west, and east flanks of the volcanic edifice, plus a repeat station at the north edge of the Crater Glacier. These stations were acquired to ascertain if there was any perched water within the edifice. Stations could not be acquired in the central core of the volcano, in the vicinity of the 1980-86 or 2004-2008 lava domes, as there is no way to make an adequate electrical connection with the ground here due to loose talus and ice. The 2011 stations are labeled MSH-1102 to MSH-1110.

Data Processing

After the CSAMT data were downloaded from the field computer system, they were examined for anisotropy and noise both visually and with software. The data were edited using the WinGLink software package in the following manner: (1) Data were evaluated to ensure that individual phase values were in the correct quadrants. (2) Data curves were smoothed using D+ (the delta function of Parker and Booker, 1996). (3) Data were checked to ensure that the rho (resistivity) values did not rise or fall steeper than 45 degrees in log-log space. The effect of this standard processing is to remove the occasional noise outliers and stack the data for the smoothest possible 1-D model fit. While data quality varied somewhat, it was acceptable. All data are reported and released in this report.

Assigning TE and TM directions

Selecting orientations for the transverse electric (TE) and transverse magnetic (TM) parts of the data is generally done with an eye to the regional structure (Vozoff, 1987). For this study, the TE orientation with electrical field oriented east would be used when operating above a north-south regional structure such as anticipated at Mount St. Helens (Weaver and others, 2012; Giampiccolo and others, 1999).

In general, AMT (including CSAMT) does not have a ready way to calculate in-phase induction orientations, as an MT sounding would, because it has no vertical magnetic reference sensor. In order to choose the prevailing strike direction and assign TE and TM, other information is required. For instance, it would require conducting galvanic vertical electrical soundings (VES) in two directions to compare the two curves or reviewing previous work, neither of which were available during the study. An MT survey across the Garibaldi Volcanic Field in the northern part of the Cascade Volcanic Arc indicated a roughly north-south crustal texture. "The induction arrows also indicate that the regional response can be characterized by a 2D resistivity model" (Jones and Dumas, 1993, p. 295). In the Washington Cascades, the motions of the Pacific, North American, and Juan De Fuca Plates control the locations of earthquakes, faults, and volcanoes. All of the most distinct features, including the subducting plate and the Washington coastline, trend roughly north-south (Weaver and others, 2012).

For an MT or AMT sounding, when the magnetic source field is parallel to the strike of the structure, this is by definition TM mode (Parker, 2010). The TE direction should thus be assigned to Zxy (XY), and TM should be assigned to Zyx (YX).

With the exception of one CSAMT station influenced by topography (station MSH-1104 at the base of the step scarp), the TE = XY orientation gave self-consistent depths, that is, Marquardt soundings are roughly similar to each other along the length of the north-south transect.

Occam Inversions

An Occam inversion generates a smooth model from CSAMT data—one different depth-conductivity value for each frequency (Constable and others, 1987). It is a fast and simple way to get a first look at the conductivity structure beneath a station, but requires a starting layer thickness and conductivity, and it cannot provide a least-squares error or other quantification of the fit. An Occam inversion of CSAMT data is shown in figure 3.

All Occam inversions were done for the TE = XY orientation. Station MSH-1001 is identical to station MSH-1002, and station MSH-1003 is identical to station MSH-1004 (two sets of repeated measurements).
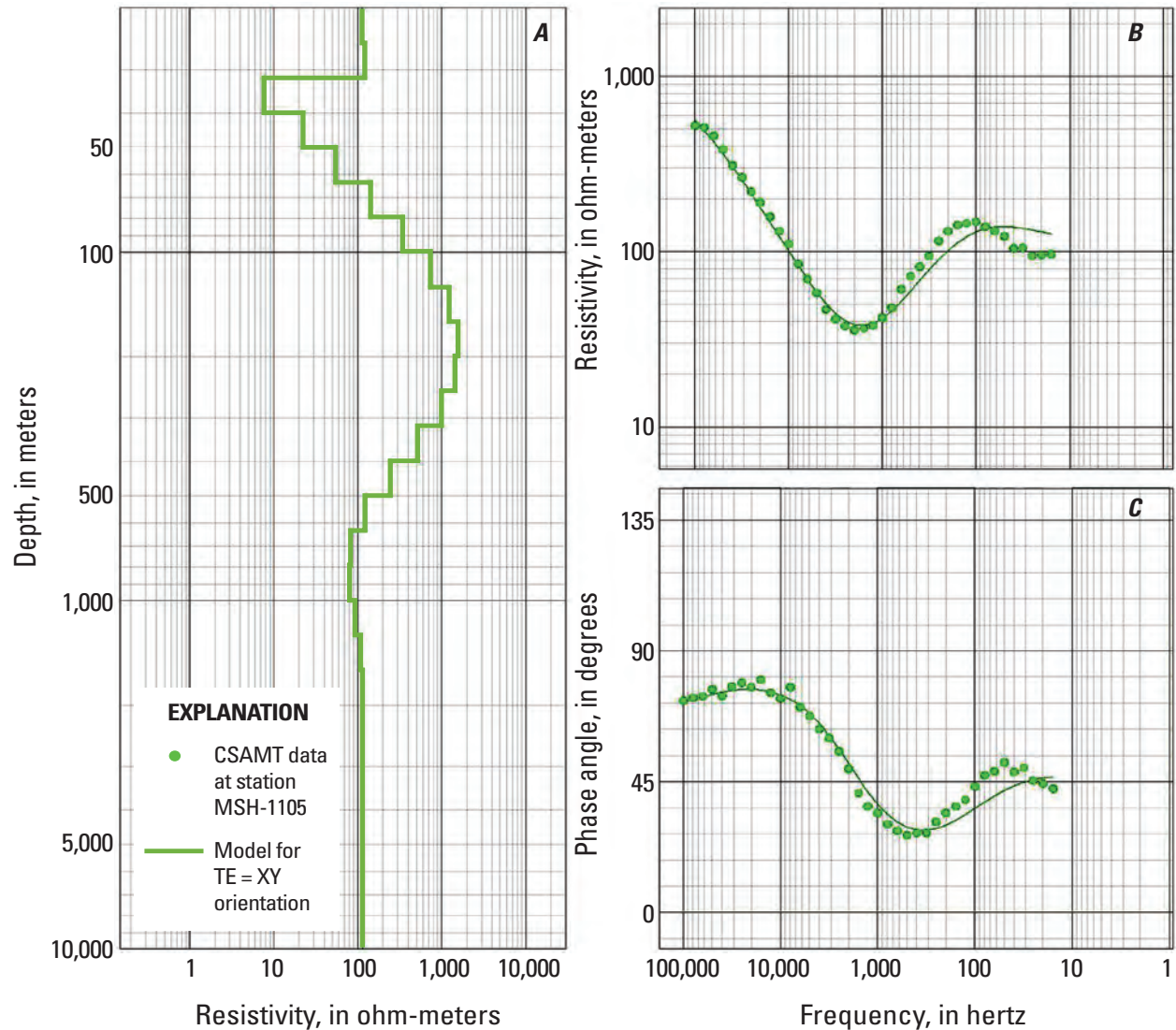
Figure 3.   Example of an Occam inversion of controlled-source audio-frequency magnetotelluric (CSAMT) data. *A*, The computer inversion of the data into a resistivity versus depth vertical profile for station MSH-1105. *B*, The original resistivity data and the inversion model fit for resistivity as a function of measurement frequency. *C*, The original phase data and the inversion model fit for phase as a function of measurement frequency.

Fischer Inversions

The singular advantage of a Fischer-type inversion is that it does not rely on a starting model. Rather, it makes direct use of the CSAMT data for information regarding layering. A typical use of the Fischer inversion is to determine how many layers can be resolved with the existing data; generally, the layers are visually obvious in the inversion (see fig. 4). These results are then used to help build a Marquardt starting model and then iterated to a true inversion (Fischer and others, 1981; Pedersen and Gharibi, 2000).

All Fischer inversions were done for the TE = XY orientation. Station MSH-1001 is identical to station MSH-1002, and station MSH-1003 is identical to station MSH-1004 (two sets of repeated measurements not duplicated here).

Marquardt Inversions

A Marquardt inversion is a damped, least-squares ridge-regression algorithm used to obtain conductivity versus depth from electromagnetic sounding data (see fig. 5). It requires a starting model that has equal to or less than the number of layers that can reasonably be observed in a Fischer inversion. The algorithm modifies the resistivities and thicknesses of the specified number of layers until it minimizes the least-squares error between the model response and the observed data. It is very sensitive to the starting (initial) model and commonly will not work if one attempts to invert for more layers than are resolved by the data (Marquardt, 1963; Pujol, 2007).

All Marquardt Inversions were done for the TE = XY orientation. If there was apparent anisotropy, the inversion was also done for TE = YX.
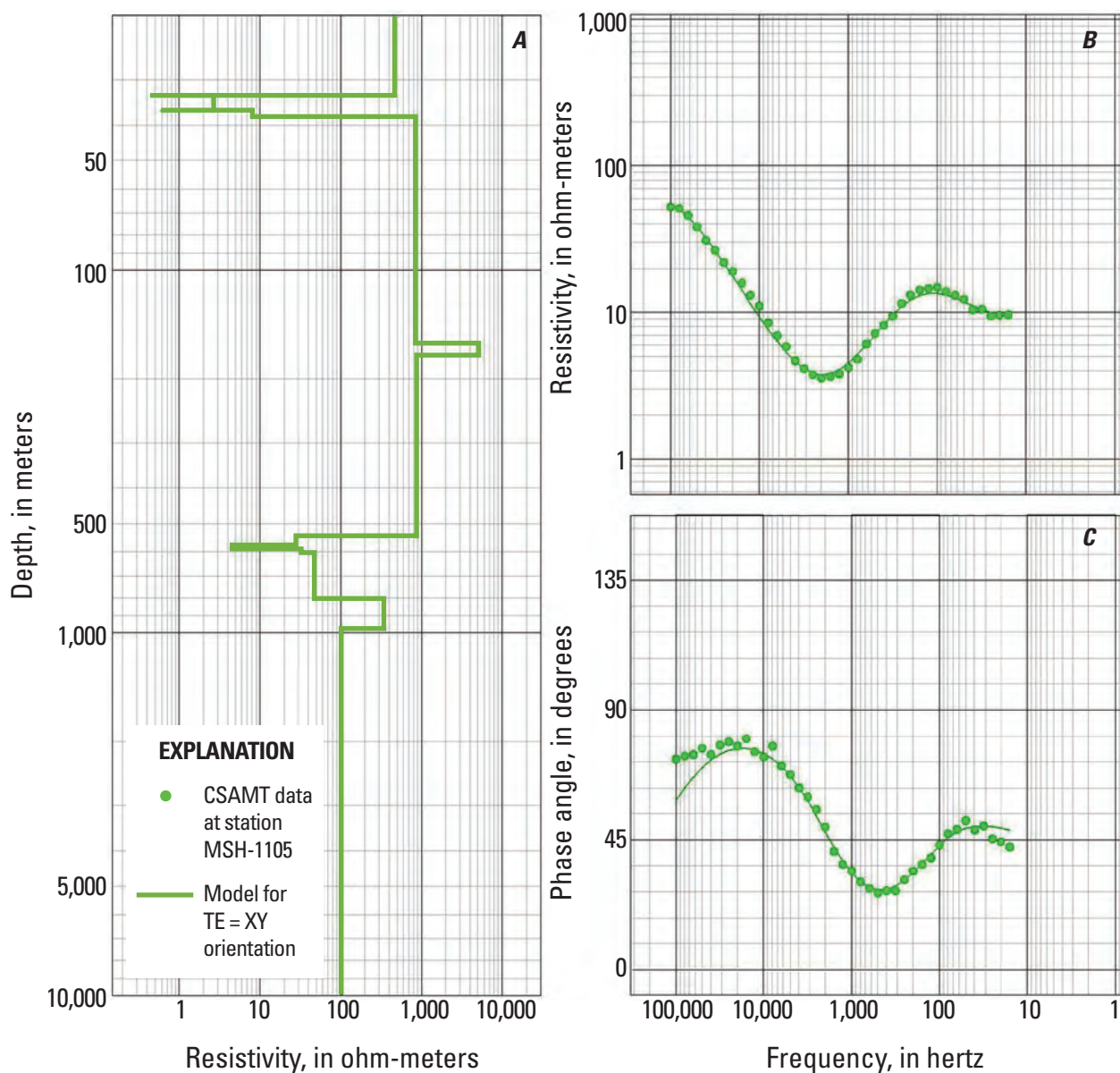
Figure 4.   Example of a Fischer Inversion of the controlled-source audio-frequency magnetotelluric (CSAMT) data. *A*, The computer inversion of the data into a resistivity versus depth vertical profile for station MSH-1105. *B*, The original resistivity data and the inversion model fit for resistivity as a function of measurement frequency. *C*, The original phase data and the inversion model fit for phase as a function of measurement frequency.

Figure 5. Example of a Marquardt Inversion of the controlled-source audio-frequency magnetotelluric (CSAMT) data. *A,* The computer inversion of the data into a resistivity versus depth vertical profile for station MSH-1105. In this figure, the separate shallow (glacier-fed) and regional aquifers are shown in light blue. *B,* The original resistivity data and the inversion model fit for resistivity as a function of measurement frequency. *C,* The original phase data and the inversion model f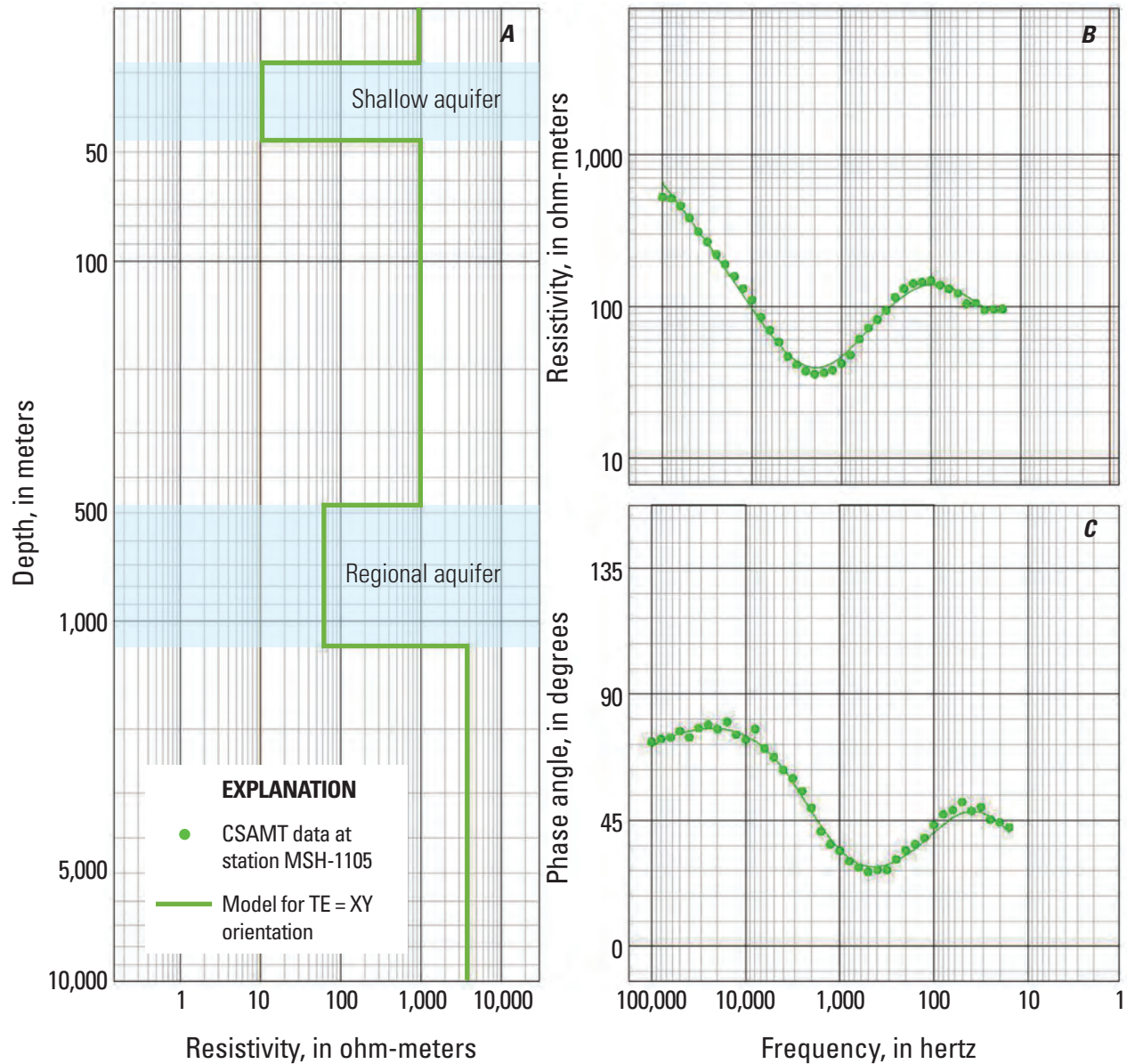it for phase as a function of measurement frequency. The fit shown between data and model in all three frames of this figure was achieved in 10 iterations, with a 0.00165 least-squares error.

References Cited

Constable, S.C., Parker, R.L., and Constable, C.G., 1987, Occam's inversion: a practical algorithm for generating smooth models from electromagnetic sounding data: Geophysics, v. 52, no. 3, p. 289–300.

Fischer, G., Schnegg, P.A., Peguiron, M., and LeQuang, B.V., 1981, An analytic one-dimensional magnetotelluric inversion scheme: Geophysical Journal of the Royal Astronomical Society, v. 67, no. 2, p. 257–278.

Geometrics, Inc., 2007, Operation manual for Stratagem [26716–01 rev. F] systems running Imagem ver. 2.19: Geometrics, Inc., 41 p., accessed July 17, 2103, at ftp:// geom.geometrics.com/pub/GeoElectric/Manuals/EH4_ manual_F.pdf.

Giampiccolo, E., Musumeci, C., Malone, S.D., Gresta, S., and Privitera, E., 1999, Seismicity and stress-tensor inversion in the central Washington Cascade Mountains: Bulletin of the Seismological Society of America, v. 89, no. 3, p. 811–821.

Jones, A.G., and Dumas, I., 1993, Electromagnetic images of a volcanic zone: Physics of the Earth and Planetary Interiors, v. 81, nos. 1–4, p. 289–314.

Kantor, Michael, and Burrows, J.H., 1996, Announcing the standard for electronic data interchange (EDI): National Institute of Standards and Technology, accessed October 11, 2012, at http://www.limswiki.org/index.php/Electronic_ data_interchange.

Keller, G.V., 1989, Electrical properties, in Carmichael, R.S., ed., Practical Handbook of Physical Properties of Rocks and Minerals: Boca Raton, Fla., CRC Press, p. 359–427.

Marquardt, Donald, 1963, An algorithm for least-squares estimation of nonlinear parameters: SIAM Journal on Applied Mathematics, v. 11, no. 2, p. 431–441.

Palacky, G.J., 1989, Resistivity characteristics of geologic targets, in Nabighian, M.N., ed., Electromagnetic Methods in Applied Geophysics Theory: Tulsa, Okla., Society of Exploration Geophysics, v. 1, p. 53–129.

Parker, R.L., 2010, Can a 2-D MT frequency response always be interpreted as a 1-D response?: Geophysical Journal International, v. 181, no. 1, p. 269–274.

Parker, R.L., and Booker, J.R., 1996, Optimal one-dimensional inversion and bounding of magnetotelluric apparent resistivity and phase measurements: Physics of the Earth and Planetary Interiors, v. 98, no. 3–4, p. 269–282, doi:10.1016/S0031-9201(96)03191-3.

Pedersen, L.B., and Gharibi, M., 2000, Automatic 1-D inversion of magnetotelluric data—finding the simplest possible model that fits the data: Geophysics, v. 65, no. 3, p. 773–782.

Pujol, Jose, 2007, The solution of nonlinear inverse problems and the Levenberg-Marquardt method: Geophysics, v. 72, no. 4, p. W1–W16.

Reid, M.E., 2004, Massive collapse of volcano edifices triggered by hydrothermal pressurization: Geology, v. 32, no. 5, p. 373–376.

Reid, M.E., Keith, T.E.C., Kayen, R.E., Iverson, N.R., Iverson, R.M., and Brien, D.L., 2010, Volcano collapse promoted by progressive strength reduction—new data from Mount St. Helens: Bulletin of Volcanology, v. 72, no. 6, p. 761–766.

Reid, M.E., Sisson, T.W., and Brien, D.L., 2001, Volcano collapse promoted by hydrothermal alteration and edifice shape, Mount Rainier, Washington: Geology, v. 29, no. 9, p. 779–782.

Schmincke, H.-U., 1998, Volcanism: Berlin, Springer-Verlag, 335 p.

Simpson, Fiona, and Bahr, Karsten, 2005, Practical magnetotellurics: Cambridge, Cambridge University Press, 254 p.

Vozoff, Keeva, 1987, The magnetotelluric method, in Nabighian, M.N., ed., Electromagnetic methods in applied geophysics, v. 1, Society of Exploration Geophysicists, Tulsa, Okla., p. 641–707.

Weaver, C.S., Grant, W.C., and Shemeta, J.E., 2012, Local crustal extension at Mount St. Helens, Washington: Journal of Geophysical Research, Solid Earth, v. 92, no. B10, p. 10,170–10,178.

Wynn, J.C., 2006, Mapping ground water in three dimensions— an analysis of airborne geophysical surveys of the upper San Pedro River Basin, Cochise County, southeastern Arizona: U.S. Geological Survey Professional Paper 1674, 33 p.

Zonge, K.L., and Hughes, L.J., 1991, Controlled source audio-frequency magnetotellurics, in Nabighian, M.N., ed., Electromagnetic Methods in Applied Geophysics, v. 2, Society of Exploration Geophysicists, Tulsa, Okla., p. 713–809.

Wynn and Pierce—**Mount St. Helens—Controlled-Source Audio-Frequency Magnetotelluric (CSAMT) Data and Inversions**—Data Series 901